Clays and Clay Minerals, Vol. 57, No. 3, 290–301, 2009.

SIMPLE SYNTHESIS AND CHARACTERIZATION OF NANOPOROUS MATERIALS FROM TALC

CHUNFANG DU AND HUAMING YANG*

Department of Inorganic Materials, School of Resources Processing and Bioengineering, Central South University, Changsha 410083, China

Abstract—Synthetic siliceous mesoporous materials are of great value in many different applications, including nanotechnology, biotechnology, information technology, and medical fields, but historically the resource materials used in their synthesis have been expensive. Recent efforts have focused on indirect synthesis methods which utilize less expensive silicate minerals as a resource material. The purpose of the present study was to investigate talc, a natural silicate mineral, as one such resource. It was used as raw material to prepare two advanced materials: porous silica (PS) and ordered mesoporous silica (MCM-41). The PS, with a specific surface area of 260 m^2/g and bimodal pore-size distribution of 1.2 nm and 3.7 nm, was prepared by grinding and subsequent acid leaching. The MCM-41, with a large surface area of 974 m^2/g and a narrow pore-size distribution of 2.8 nm, was obtained using a surfactant, cetyltrimethylammonium bromide (CTAB), by hydrothermal treatment using the as-prepared PS as a source of Si. The two resultant materials were characterized by small angle X-ray diffraction (SAXRD) and wide-angle X-ray diffraction (WAXRD), high-resolution transmission electron microscopy (HRTEM), solid-state magic-angle-spinning nuclear magnetic resonance (MAS NMR), Fourier transform infrared spectroscopy (FTIR), and N_2 adsorption-desorption measurements. Based on these measurements, possible processes of transformation of PS from talc, upon acid treatment, and the formation of MCM-41 were investigated systemically. Acid leaching induced the transformation of a rigid layered structure to a nearly amorphous one, with micropores formed by a residual layered structure and mesopores formed from a condensed framework. The MCM-41 was a mixture of silanol groups ($Si(SiO)_3(OH)$) and a condensed Q^4 framework structure ($Si(SiO)_4$), with a small amount of remaining Q^3 layered structure ($Si(SiO)_3OMg$). The increased Q^4/Q^3 value confirmed greater polymerization of MCM-41 than of PS. At the low CTAB concentration used (2 wt.%), the highly charged silicate species controlled the surfactant geometry. Charge-density matching, together with the degree of polymerization of the silicates, determined the resultant mesophase.

Key Words—Acid Leaching, Grinding, Hydrothermal Treatment, Mesoporous Silica, Nanoporous Silica, Silicate Minerals, Talc.

INTRODUCTION

Considerable progress has been made in the field of porous materials due to the increase in the number of applications in, for example, catalysis supports for adsorption, phase separation, fuel-cell electrodes, drug delivery, ion exchange, *etc*. (Corma, 1997; Vallet-Regi *et al.*, 2001; Davis, 2002; Mukhopadhyay *et al.*, 2002; Coasne *et al.*, 2006; Warren *et al.*, 2008). In particular, the siliceous mesoporous materials such as MCM-41, MCM-48, and SBA-15 (Kresge *et al.*, 1992; Beck *et al.*, 1992; Zhao *et al.*, 1998) have garnered a great deal of attention because of their highly ordered structures, ultra-large surface areas, narrow pore-size distributions in the mesopore range, and tunable pore sizes (2−50 nm), which can lead to superior properties and applications. These materials can be assembled by a template mechanism involving the formation of surfactants of block copolymer micelles in a mixture containing a solvent and a source of Si. To date, however, most strategies involved in the assembly of siliceous mesoporous materials have concentrated on direct synthesis by choosing certain soluble Si sources including organic or inorganic reagents, such as tetraethyl orthosilicate (TEOS) and water glass (Xu *et al.*, 1998; Mokaya, 1999; Boissière *et al.*, 2000; Pauly *et al.*, 2002; Kosuge *et al.*, 2004). The main drawback with this procedure is the need for very expensive sources of Si which challenges the practical applications of siliceous mesoporous materials.

To circumvent this problem, many researchers have investigated possible indirect synthesis using silicate minerals. For example, a highly ordered mesoporous FSM-16 material was fabricated from a layered polysilicate (Inagaki *et al.*, 1993). In this case, a mesoporous silica with uniform pore size was prepared by ion exchange of surfactants for the interlayer Na ions in the layered polysilicate, kanemite. Silicate minerals can thus be used as sources of Si to prepare mesoporous materials, thereby upgrading low-cost substances to valuable products.

In recent years, acid leaching of silicate minerals such as talc, kaolin, antigorite, sepiolite, vermiculite,

* E-mail address of corresponding author:
hmyang9392@hotmail.com
DOI: 10.1346/CCMN.2009.0570302

pyrophyllite, chlorite, phlogopite, *etc.* in order to obtain PS (Kosuge *et al.*, 1995; Aznar *et al.*, 1996; Okada *et al.*, 1998, 2002, 2005; Temuujin *et al.*, 2003a, 2003b; Yang *et al.*, 2006) has attracted much attention because of the low cost and simple process, as well as the broad pore-size distribution of the products, and because of the ready availability of the raw materials. The process involves dissolution of cations, *e.g.* Mg,Al in octahedral sites and Al,Fe in tetrahedral sites, from a crystal framework and the formation of amorphous, hydrated silica with complete or incomplete breakdown of the original structure. On the other hand, PS has been used as a raw material in the manufacture of mesoporous materials (Linssen *et al.*, 2003; Miao *et al.*, 2005; Madhusoodana *et al.*, 2006). The transformation from silicate minerals to PS and highly ordered mesoporous silica materials is achieved by means of acid-leaching treatment and a surfactant-assisted template method on clay minerals. In other words, 'one common source, two advanced materials' can be realized, which will bring benefits to applications in nanotechnology, biotechnology, information technology, and medical fields.

Talc, a 2:1 layered silicate with one octahedral sheet sandwiched between two tetrahedral sheets, was selected to prepare PS which was then used as a source of Si to fabricate the ordered mesoporous material MCM-41 in the presence of a surfactant (CTAB).

EXPERIMENTAL

Materials

Talc from Guilin, China, was used as the raw material. The chemical composition (wt.%) was 62.45 SiO_2, 31.16 MgO, 0.63 Fe_2O_3, 0.08 Al_2O_3, and 0.1 TiO_2. Other reagents were used without purification.

Synthesis of PS

Silicates are rigid structured minerals, which mainly encompass Si-O or Al-O tetrahedra, Al-O and/or Mg-O octahedra. Talc consists mainly of Si-O tetrahedra and Mg-O octahedra. Two processes were involved in the synthesis of PS from talc. Grinding is essential for talc (but unnecessary for other samples) because of its compact structure and lack of substitution in tetrahedral and octahedral sites. Reduction in particle size and destruction of the framework structure were both achieved by grinding. Acid leaching is also critical; it eliminates impurities, leading to PS with large Si contents. For talc, Mg^{2+} in the octahedral sites needed to be removed, for which hydrochloric acid (HCl) was used as the leaching reagent.

Talc was ground in a planetary mill (KM-10 planetary mill, Nanjing University Instrument Plant, China) at 800 rpm for 6 h with a ball-to-sample weight ratio of 10:1. The ground sample (10 g) was treated with 200 mL of 6 M HCl at 80ºC for 2 h. The suspension was then washed with distilled water several times to remove Cl^- and then dried at 80ºC for 12 h. Finally, PS was obtained.

Synthesis of MCM-41 from PS

The PS, obtained from acid leaching of the talc, was used as the source of Si to synthesize the mesoporous material MCM-41. In a typical procedure, 10 g of PS was added to a cetyltrimethylammonium bromide (CTAB) solution. A well-controlled NaOH solution (0.5 M) was added dropwise in order to adjust the pH of the mixture to 12.0. The mixture was then transferred to a Teflon-lined steel autoclave and statically heated at 100ºC for 24 h after stirring for 2 h at 60ºC. The resultant white product was filtered, washed several times with deionized water, dried at 80ºC overnight, and then calcined at 540ºC in air for 6 h with a heating rate of 2ºC/min in a SK2-2-12 type tube furnace. Finally, the MCM-41 material was obtained.

Characterization

The XRD patterns were recorded using a Rigaku D/max 2550 using CuKα radiation (λ = 0.15406 nm) over the scanning range of ~1−10º2θ for SAXRD at a voltage of 40 kV and current of 300 mA, and over the range ~10−90º2θ for WAXRD at a voltage of 40 kV and 200 mA, both with a step size of 0.02º2θ. Nitrogen gas adsorption-desorption isotherms were measured at 77 K using an ASAP 2020 unit. Prior to the sorption experiment, the materials were dehydrated by evacuation under specific conditions (200ºC, 10 h). The specific surface area was calculated by the Brunauer-Emmet-Teller (BET) method and the pore-size distribution was calculated by the Barrett-Joyner-Halenda (BJH) method for MCM-41 and by the BJH and Horvath-Kawazow (HK) methods for PS, using the desorption isotherm, respectively. The total pore volume was obtained from the maximum amount of nitrogen gas adsorbed at partial pressure (p/p_0 = 0.999). High-resolution transmission electron microscopy images were captured using a JEM-2010 electron microscope operated at 200 kV. The PS and MCM-41 samples were dispersed ultrasonically in ethanol and held for 15 min. A drop of suspension was then dripped onto a copper grid and allowed to dry. Fourier transform infrared spectra were recorded on a Shimadzu FTIR 8120 spectrometer using the dried KBr disc technique, over the range ~4000−400 cm^{-1}. The ^{29}Si MAS NMR spectra were recorded using a Varian Infinityplus 300 MHz spectrometer at 7.0 T in order to characterize the local structure around the Si atoms in the samples.

RESULTS AND DISCUSSION

The SAXRD patterns and HRTEM images (insert) of PS and MCM-41 (Figure 1) revealed no obvious diffraction peak for PS (Figure 1a), indicating the disordered structure. Four distinct diffraction peaks, however, could

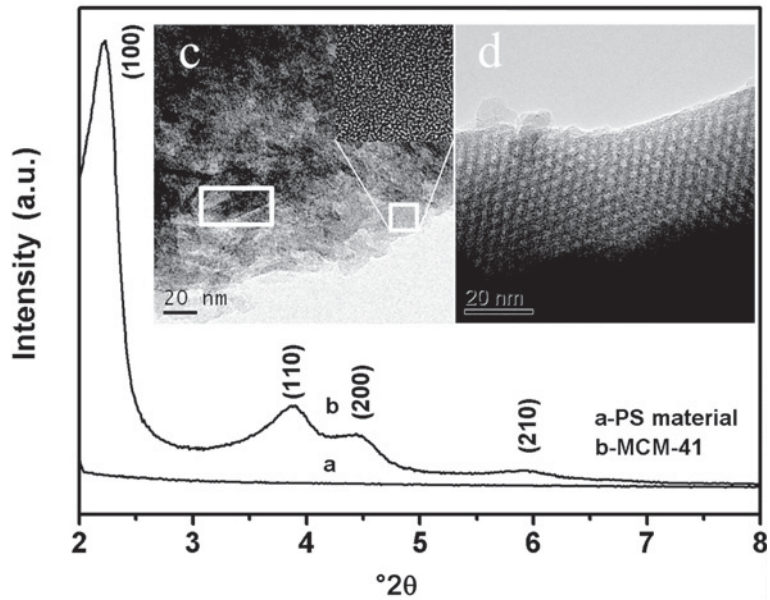

Figure 1. SAXRD patterns and HRTEM images of PS and MCM-41 (PS material: a, c; MCM-41: b, d).

be indexed readily to MCM-41 (Figure 1b), demonstrating the regular mesoporous structure, which was further confirmed by HRTEM images.

The HRTEM images of PS and MCM-41 were used to study the transformation of the structure upon acid treatment and after the template-assisted process. The TEM image of PS showed a nearly amorphous structure (magnified inset of Figure 1c) with a small amount of residual layered structure. This result was similar to that for saponite (Bisio *et al.*, 2008), the morphology of which was not modified dramatically under acid treatment with the lamellar (smectitic) structure being almost lost. These phenomena were attributed to the different leaching conditions, especially the variation of leaching temperature and concentration of leaching reagent. The greater acid concentration and temperature led to the collapse of the crystalline structure (Linssen *et al.*, 2002). An amorphous material, containing only Si (because of acid leaching), is not necessarily the ideal source of Si to use to prepare ordered, mesoporous MCM-41 with maximum specific surface area. For mesoporous silica prepared using acid-treated saponite as the source of Si (Okada *et al.*, 2007), the maximum specific surface area obtained was not from the Si source with pure silica, but from that with a certain Si/(Mg+Al) ratio. The effects of linkage structure of SiO_4 tetrahedra and the residual octahedral Al and Mg ions in the precursors were suggested to be possible reasons. Compared with PS, MCM-41 exhibited distinctly ordered mesopores (Figure 1d). The lack of similarity in terms of porous structure between PS and MCM-41 results from the participation of the surfactant (CTAB), a structure-determining agent (SDA) or template which played an important role in the formation of ordered mesoporous materials.

The WAXRD patterns of the samples (Figure 2) indicate that grinding destroyed the rigid structure of the talc and reduced it to a nearly amorphous material. The leaching treatment, however, had no obvious effect on the structure of the ground talc. The PS from the acid leaching of the ground sample was nearly amorphous with a small amount of residual layered structure from the talc, in accord with the HRTEM analysis. The resultant product, MCM-41, was a completely X-ray amorphous SiO_2.

N_2 adsorption-desorption measurement is a useful tool to characterize porous materials. The N_2 adsorption-desorption isotherms and pore-size distribution curves of raw talc after leaching (RTL), of PS, and of MCM-41 (Figure 3, Table 1) found that the isotherm shapes of the

Table 1. Sample data from N_2 adsorption-desorption isotherms and pore-size distribution curves.

Samples	S_{BET} (m^2/g)	Types of isotherm	Types of hysteresis loop	Pore volume (cm^3/g)	Pore size (nm)
RTL material	3	II	–	0.01	–
PS material	260	I, II and IV	H3 and H4	0.51	1.2 and 3.7
MCM-41	974	IV	H1	1.00	2.8

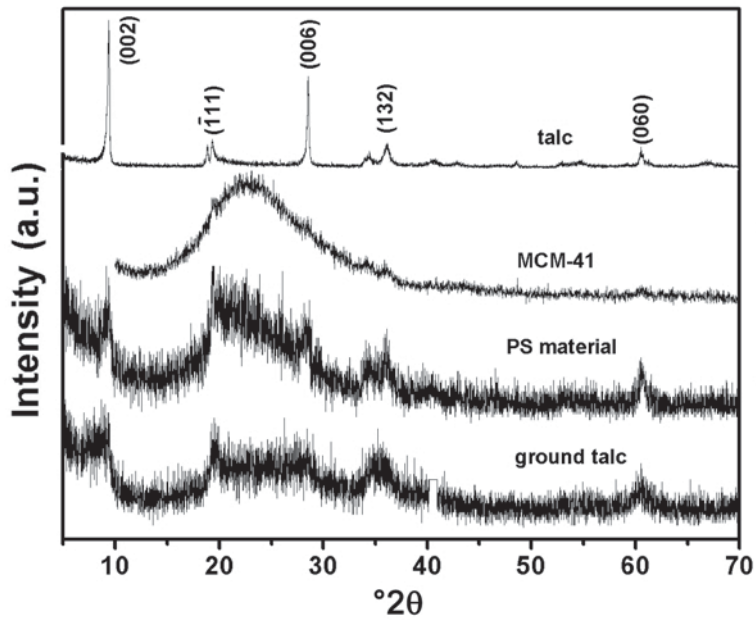

Figure 2. WAXRD patterns of talc, ground talc, PS, and MCM-41 materials.

three samples are different. The RTL material had almost no adsorption, with a representative isotherm of type II. The lack of a clear peak in the pore-size distribution confirmed the non-porous state of the RTL material. Grinding is a critical part of the process by which PS is created. Grinding for a short period reduced the particle size of talc. For longer grinding times, however, an intense degradation of the structure and loss of the lamellar shape was observed, along with a progressive amorphization with the formation of hard agglomerates. For talc, the rigid structure with no substitution in either the tetrahedral or octahedral sites and layer surfaces containing oxygen atoms with hydrophobic characteristics (Temuujin *et al.*, 2002) are believed to be the main reasons for its slow leaching behavior, small surface area (3 m^2/g), and small pore volume (0.01 cm^3/g) (Table 1). After grinding, the acid-leaching product had a larger surface area and a larger

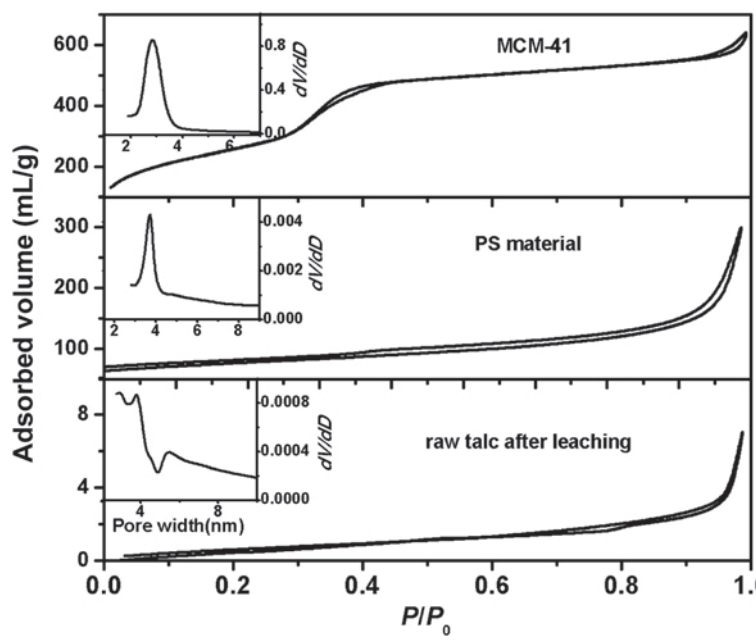

Figure 3. N_2 adsorption-desorption isotherms and pore-size-distribution curves of RTL, PS, and MCM-41 materials.

pore volume, nearly 86 times and 50 times that of RTL material, respectively. The effects of grinding on the preparation of PS from vermiculite (Maqueda *et al.*, 2007) and talc (Temuujin *et al.*, 2002) were investigated and the same results obtained. Grinding promotes the leaching behavior of clay minerals, enlarging the surface area and pore volume of the resultant products to 186 m^2/g and 0.53 cm^3/g, respectively, for leached talc after grinding, ~10 times and 8 times as much as the un-ground version (Temuujin *et al.*, 2002). After grinding, the surface area and pore volume of leached vermiculite were 720 m^2/g and 0.59 cm^3/g, respectively, ~1.5 times and approximately the same, as the un-ground version, respectively (Maqueda *et al.*, 2007). The enhancement of specific surface area and pore volume for talc was apparently more extensive than that of vermiculite, although the resultant specific surface area of the former was much less than that of the latter. Comparing the original structures of the two clay minerals, this discrepancy could be attributed to the substitution which occurred in the tetrahedral and octahedral sites in vermiculite, which was responsible for the easy leaching of raw material and the greater surface area and pore volume achieved. The compact crystal structure of talc inhibited the dissolution of Mg^{2+} from octahedral sites, which resulted in the smaller surface area and pore volume, and allowed increased porosity after grinding.

The leaching behavior, however, did not appear to be consistent with the grinding time, *e.g.* the preserved leached cation (Mg^{2+}) content did not decrease with grinding time (Yang *et al.*, 2006). In the case of pyrophyllite (Temuujin *et al.*, 2003b), this phenomenon was ascribed to either the presence of strong Al−O−Si bonds, through conversion of octahedral Al to tetrahedral coordination, which impedes Al leaching, or an agglomerated particle structure generated by increasing surface energy with increased grinding time. Compared with pyrophyllite, Mg^{2+} rather than Al^{3+} was present in the octahedral sites, indicating the absence of Al−O−Si bonds. The agglomeration among particles was, therefore, the main cause of the leached cation content not reaching a minimum with increased grinding time.

The PS isotherm was a mixture of types II and IV, with an initial portion resembling a type I isotherm and a hysteresis loop mixture of H3 and H4, indicative of narrow slit-shaped pores. The pore-size distribution was bimodal, 1.2 nm in the microporous region (not shown) calculated using the HK method and 3.7 nm in the mesoporous region, calculated using the BJH method. This result was much different from that of other samples (Temuujin *et al.*, 2002), where a characteristic, sharp pore-size distribution was absent. This dissimilarity could be ascribed to the different grinding and leaching conditions, where grinding may not be sufficient to produce a fully amorphous structure and the leaching was not adequate to completely remove Mg^{2+}. Based on previous studies (Okada *et al.*, 2002; Temuujin *et al.*, 2002, 2003a; MacKenzie *et al.*, 2004), the micropores were formed by the tetrahedral sheets between the removed octahedral sheets and the micropore size might correspond to the space left by removal of the octahedral sheets. The micropore size in acid-treated vermiculite and phlogopite corresponded to the space left by removal of the octahedral sheets (Okada *et al.*, 2002; Temuujin *et al.*, 2003a). The micropore size (1.2 nm) of acid-leached talc, however, was much larger than the space left after removal of the octahedral sheets. The difference between the pore size and the basal spacing of the original layered structure may result from structure distortion (Temuujin *et al.*, 2001a). Compared with the other two 2:1 type layered silicates (Okada *et al.*, 1998, 2002, 2005; Temuujin *et al.*, 2003a; MacKenzie *et al.*, 2004), the main difference in the synthetic process was the adoption of pre-treatment for raw materials, *i.e.* manipulation of talc grinding before acid treatment, which resulted in the different porosity properties from the counterpart under different pre-treatment (Okada *et al.*, 2003). PS prepared from kaolin was activated in two ways: calcination and mechano-chemical treatment (Okada *et al.*, 1998; Temuujin *et al.*, 2001b), which resulted in a discrepancy in micropore size. The calcination, preserving the original layered structure, was responsible for the micropores with a constant pore size (0.6 nm) formed in the process of acid leaching, while the mechano-chemical treatment, leading to structure distortion, caused the pore size of ~3.8 nm and some smaller micropores which changed with prolonged leaching time. The possible changes generated in the interlayers of mechanically treated talc, included gliding caused by a shearing effect, accompanied by the rupture of some interlayer bonds, may be the cause of the micropore size being larger than the basal spacing of the original layered structure. Different pre-treatment of raw materials could produce a discrepancy in their micropore-size distribution even for the same type of layered structure.

Two main mechanisms have been proposed to explain the formation of PS from 2:1 layered silicates, including edge-attack and gallery-access mechanisms (Kaviratna and Pinnavaia, 1994). The edge-attack mechanism is predominant in leaching of 2:1 layered silicates, whether the starting material is swelling clay or non-swelling clay. Substitution occurring in tetrahedral sheets opens up the pathways for acid attack on the octahedra and interlayers by both gallery access and edge access, enhancing the degree of selective leaching of the starting materials. Talc is a non-swelling clay with no substitution in the tetrahedral sheets. The edge-access mechanism, therefore, is mainly responsible for the leaching behavior of talc although most of the 2:1 type clay minerals are of the gallery access type.

The mesopores probably resulted from the formation of a framework structure by the rearrangement and condensation of silica tetrahedra. The mesopore size

increased with extended leaching time (Okada *et al.*, 2002; Yang *et al.*, 2006). This tendency was analogous to that of vermiculite and phlogopite (Okada *et al.*, 2002; Temuujin *et al.*, 2003a), but unlike that of kaolin (Temuujin *et al.*, 2001a). The variation in mesopore size with leaching time being remarkably different could be attributed to the different residual SiO_4 tetrahedra in the 2:1 and 1:1 layered structures (Okada *et al.*, 2002). In the 2:1 layered structure, the active oxygens of the SiO_4 tetrahedral sheets formed by selective leaching of the Mg octahedral sheets face each other, and condense readily to form a framework structure. For the SiO_4 tetrahedral sheets substituted by AlO_4, the leaching of Al in tetrahedral sites greatly promotes the rearrangement of the residual layered structure to form a framework structure. For a 1:1 layered structure, the apical oxygens face the same direction after acid leaching of the Al octahedra. This structure holds back the condensation of Si-O tetrahedra to a certain degree, and results in no obvious variation in mesopore size with prolonged leaching time irrespective of any pre-treatment adopted.

The shape of the N_2 adsorption-desorption isotherm of MCM-41was a typical IV type isotherm, corresponding to mesoporous materials. The sharp inflection between the relative pressures p/p_0 = 0.3−0.4 in the isotherm corresponded to capillary condensation within uniform mesopores. The sharpness of this step demonstrated the uniform pore-size distribution, which was confirmed by the pore-size distribution curve. In contrast to the great amount of adsorption of N_2 in the region of ~0.3−0.4, a slight increase in the range $0.4 \leqslant p/p_0 \leqslant 0.95$ was observed, which indicated that mesopores with pore size >2.8 nm could be ignored. The increase in the vicinity of p/p_0 near 1.0 could be ascribed to the presence of macropores corresponding to the spaces formed by agglomeration of the mesoporous particles (Okada *et al.*, 2007). The small hysteresis in whole ranges of adsorption and desorption isotherms suggested the cylindrical, straight, and uniform mesopores without a distinct throat. An ordered mesoporous material with large surface area (974 m^2/g) and uniform pore-size distribution (2.8 nm) could be obtained using PS which originated from talc as the source of Si. The mesoporous material obtained was very similar to that prepared by the direct synthesis method using chemical reagents (Xu *et al.*, 1998; Mokaya, 1999; Boissière *et al.*, 2000; Pauly *et al.*, 2002; Kosuge *et al.*, 2004).

Solid-state NMR is powerful at detecting the chemical environment of various atoms. Recently, it has been used in the characterization of ordered mesoporous silica, including structure, relative concentration, and the location and reactivity of various anchored groups in functionalized mesoporous silicas (Trébosc *et al.*, 2005; Azaïs *et al.*, 2006; Baccile *et al.*, 2007; Shenderovich *et al.*, 2007; Cai *et al.*, 2007). The ^{29}Si MAS NMR spectra of the samples indicated the progressive transformation of the raw talc to PS, and then to ordered MCM-41 (Figure 4). The chemical shift of raw talc was at −97 ppm which corresponds with previous results (Kinsey *et al.*, 1985), with an upshift from −100 to

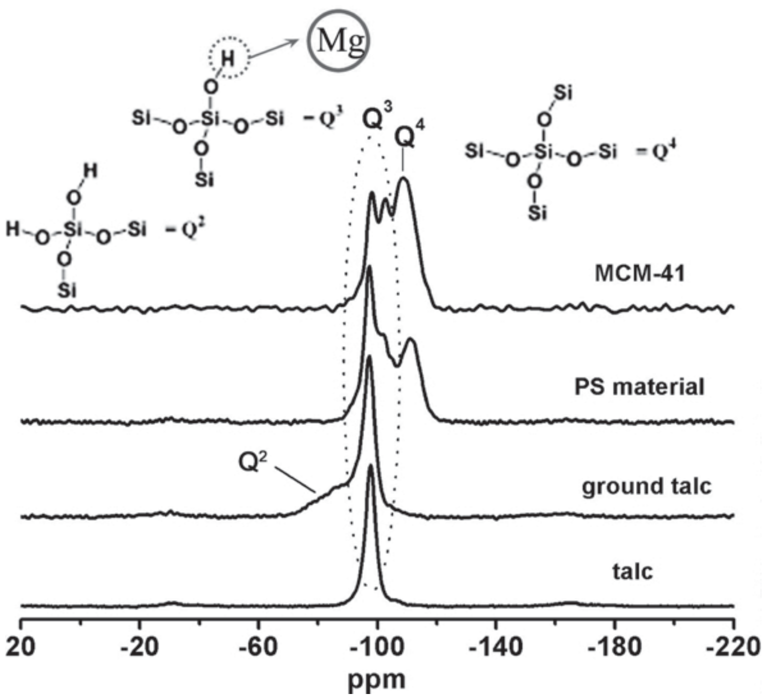

Figure 4. ^{29}Si NMR spectra.

−97 ppm compared with silanol groups ($Si(SiO)_3(OH)$) because of the edge link of Mg atoms rather than H atoms. A new shoulder located in the range of −90 to −70 ppm after grinding was attributed to silicon Q^2 ($Si(SiO)_2(OH)_2$) sites. The DTA result of ground talc demonstrated that enstatite was formed from amorphous talc during grinding (Sánchez-Soto *et al.*, 1997). The formation of enstatite required only a slight displacement of the cations within the fragment of the Mg-O-H layer, which was altered by structural alteration during the grinding process. The new shoulder was therefore ascribed to the Q^2 structure of enstatite. The involvement of foreign atoms had great influence on the chemical environment of Si atoms. After leaching, two new resonances located at −102 ppm and −111 ppm emerged, which could be assigned to silicon Q^3 ($Si(SiO)_3(OH)$) and Q^4 ($Si(SiO)_4$) sites, respectively. The emergence of a chemical shift at −102 ppm demonstrated the partial transformation from $Si(SiO)_3OMg$ to $Si(SiO)_3(OH)$, *i.e.* H atoms replaced Mg atoms during the acid-leaching process, which could be further verified by FTIR spectra (Figure 5). The chemical shift changing from −97 ppm to −102 ppm for Q^3 structure was attributed to the smaller electron cloud density of H atoms than Mg atoms. The residual Si-O framework after removing Mg^{2+} continued to condense and promoted the formation of amorphous SiO_2, a three-dimensionally bonded four-coordinated silicon which was responsible for the presence of −111 ppm in NMR spectra. The existence of a chemical shift at −97 ppm after leaching indicated a preservation of the layered Q^3 structure, which was consistent with the WAXRD and HRTEM results. Based on the results from NMR spectra and the pore-size distribution curve, the PS structure is suggested to consist of micropores formed from a residual layered part and mesopores formed from a condensed framework part. This result was consistent with that of phlogopite (Okada *et al.*, 2002) and kaolinite (Okada *et al.*, 1998). SiO_4 sheets were not scrapped even in the case of amorphous silica with very small MgO contents because Q^2 units were not observed in the ^{29}Si NMR spectra of PS (Kosuge *et al.*, 1995). The same result was obtained in the NMR spectra of talc (Figure 4). In the case of sepiolite (Jin *et al.*, 2007), three similar chemical shift peaks were displayed in the NMR spectra, besides a peak located at −87 ppm which was attributed to the inherent Q^2 unit of sepiolite. A reasonably clear ^{29}Si NMR spectrum, therefore, would be obtained from acid leaching of various silicates, taking no account of the differences which resulted from intrinsic dissimilarities in their raw structures.

Unlike other counterparts, three distinct peaks were located at −98, −102, and −108 ppm in the NMR spectra of calcined MCM-41. Taking the origin of the Si source into account, the residual Mg^{2+} content after the acid leaching was the key point for the existence of the peak at −98 ppm, suggesting the preserved layered structure of talc. The other peak belonging to a Q^3 configuration located at −102 ppm was unambiguously attributed to $Si(SiO)_3(OH)$. The ^{29}Si chemical shift is highly sensitive to the mean bond length of SiO (d_{SiO}) and Si−O−Si bond angle (α), with downfield shifts at greater d_{SiO} and smaller α values (Kosuge *et al.*, 1995). The downfield shift in the Q^3 unit from −93 to −90 ppm in the ^{29}Si NMR spectra of acid-leached antigorite was mainly attributed to the decrease in α, which was generated by the variation of the corrugated layers with periodic inversion of the SiO_4 tetrahedra of the original antigorite to flattening layers upon Mg^{2+} dissolution (Kosuge *et al.*, 1995). In comparison, talc has flattening layers other than the serpentine layers, so no obvious chemical shift was expected in the inherent Q^3 unit

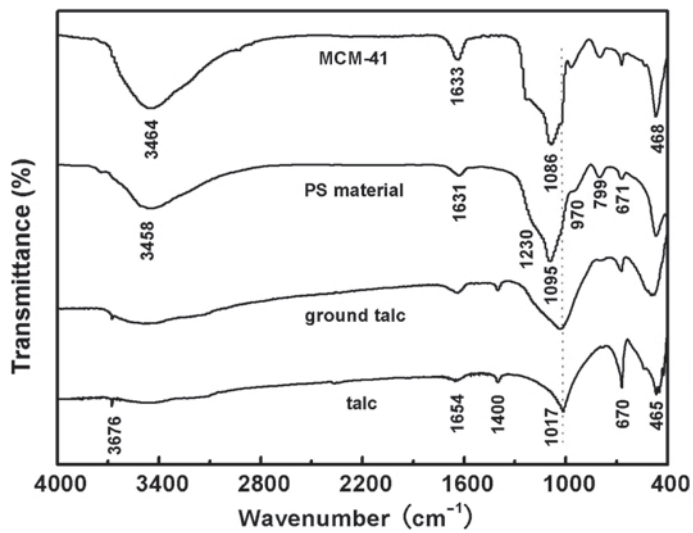

Figure 5. FTIR spectra.

during the acid-leaching process from raw talc to amorphous silica. A visible upshift for the Q^4 unit, however, was observed after the ordering process. Based on the established correlations between chemical shift and α, the peak upshift from -111 to -108 ppm could be related to the decrease in the α value.

The Q^4/Q^3 ratio of the framework from the peak area of the ^{29}Si NMR spectra could be calculated according to the following equation (Jin *et al.*, 2007):

$$Q^4/Q^3 = S_Q^4/S_Q^3$$

where S_Q^4 is the fraction of peak area of the Q^4 silica configuration and S_Q^3 is the fraction of peak area of the Q^3 silica configuration. All spectra were simulated and separated using the Gaussian model, giving fractions of the peak area of various Si configurations based on the simulated lines (Table 2).

After acid leaching, the silanol structure $Si(SiO)_3(OH)$ emerged and condensed to form a Q^4 unit. The Q^4/Q^3 ratio of MCM-41 increased compared with PS, which demonstrated a greater degree of polymerization of the Si-O structure in ordered MCM-41.

An analysis of the FTIR spectra was carried out to check the effects of grinding and acid leaching on the structural evolution from talc to PS, as well as the ordered mesoporous MCM-41, presenting the distinctions between PS and MCM-41. Two characteristic parts were displayed in the FTIR spectra (Figure 5). The broad band in the range ~3750–3400 cm^{-1} could be assigned to the surface structural hydroxyl groups of the layered aluminosilicates as well as the adsorbed water. A series of bands located at ~1400–400 cm^{-1} could be attributed to the lattice vibration of the clay minerals.

Grinding had obvious effects on the structural variation of talc. The sharp lines at 3676 and 670 cm^{-1} were related to the typical vibration of the Mg-OH band. The decreased intensity of the band indicated the weakness of the Mg–OH bond, which helped with leaching.

Acid leaching induced the transformation from Si-OMg bands into Si-OH bands, and resulted in the collapse of structure and conversion of the crystalline structure into hydrated silica, which were verified by the following aspects: (1) the increased intensity of the bands belonged to the adsorbed water (3458 and 1631 cm^{-1}); (2) the emergence of shoulders at 1230 and 970 cm^{-1} assigned to a free-silica stretching vibration (Suquet, 1989; Vicente *et al.*, 1996); (3) the decreased intensity of the Mg-OH bending vibration at 671 cm^{-1} and the complete absence of the band attributed to the Mg-OH stretching vibration; and (4) the formation of a new band oriented at 799 cm^{-1} attributed to Si-OH vibration (Suquet, 1989). A notable peak shifted from 1017 cm^{-1} in talc to 1095 cm^{-1} in PS without perceptible shift after grinding. The former band (1017 cm^{-1}) corresponded to an in-plane Si-O stretching vibration and the latter (1095 cm^{-1}) corresponded to an out-of-plane Si-O stretching vibration. The active oxygen atoms in Si-O tetrahedra of talc linked not only to Si atoms but also to Mg atoms residing in octahedral sites. Thus, in-plane stretching was the main vibration mode for Si–O bonds in the original crystalline structure. Releasing Mg^{2+} from the octahedral sites in talc gave rise to out-of-plane stretching vibrations of Si-O bands which were located at 1095 cm^{-1}. Peak shifts in the FTIR spectra were mostly related to differences in atomic mass and bond strength (Lubguban *et al.*, 2000). The blue shift of Si-O bands in FTIR spectra can only be related to the Si–O bond strength. As a consequence of acid leaching, the sites occupied by Mg atoms were substituted by H atoms, the electronegativities of which were mostly smaller than Mg atoms. The increased strength of the Si–O bonds, therefore, resulted in the blue shift of the Si–O stretching bond. This result was in accord with the results from the ^{29}Si NMR spectra. MCM-41 had a very similar IR spectrum to the other samples reported previously, ignoring the band at 670 cm^{-1} which was assigned to the vibration of preserved Mg-OH bands.

Based on adsorption-desorption data, NMR and FTIR results, and other models (Kosuge *et al.*, 1995; Maqueda *et al.*, 2007), a possible process for PS formation from talc through acid treatment is proposed and summarized schematically (Figure 6) by illustrating a representative 2:1 type clay structure consisting of an octahedral sheet sandwiched between two tetrahedral sheets. The schematic shows a limited region and not the whole. By eliminating the octahedral sheets, new surfaces arise, facing each other (Figure 6b). These new surfaces, with large numbers of silanol groups, were partly responsible for the increase in surface area and are reactive to form a Si-O framework (Kosuge *et al.*, 1995). Three distinguishing structures are presented (Figure 6c): region A was responsible for the chemical shift at -97 ppm shown

Table 2. ^{29}Si NMR results of the samples obtained.

Samples	Peak locations for Q^3 units (ppm)	Peak location for Q^4 unit (ppm)	Q^4/Q^3
Talc	−97	–	–
Ground talc	−97	–	–
PS material	−97, −102	−111	0.66
MCM-41	−98, −102	−108	1.84

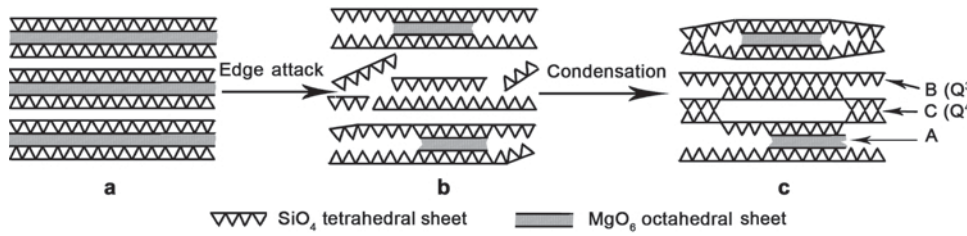

Figure 6. Schematic model of the possible formation of PS from talc.

in ^{29}Si NMR spectra, a residual layered piece of talc; region B gave the chemical shift at −102 ppm for the Q^3 ($Si(SiO)_3(OH)$) structure, indicating that Si atoms bearing OH groups were formed upon acid treatment; and region C gave the chemical shift at −111 ppm for the Q^4 ($Si(SiO)_4$) structure with a three-dimensional cross-linked framework which originated from the condensation of the hydroxyl groups and formation of siloxane bonds.

After adding PS to the solution containing CTAB, the resultant ordered mesoporous material, MCM-41, was obtained by adjusting the pH. For the synthesis of mesoporous material, many mechanisms have been proposed to interpret this interesting process (Yanagisawa *et al.*, 1990; Kresge *et al.*, 1992; Beck *et al.*, 1992; Inagaki *et al.*, 1993; Monnier *et al.*, 1993; Huo *et al.*, 1994a, 1994b; Firouzi *et al.*, 1995). Among them, a liquid-crystal templating (LCT) mechanism was first proposed which acted as a combination of other mechanisms, and thus was popularly adopted. Two pathways were proposed, under the LCT mechanism, to explain the formation of ordered mesoporous materials. In the first pathway, a micellar rod around the surfactant micelle was initially formed, which would produce an hexagonal array of rods, followed by incorporation of an inorganic array (silica, silica-alumina) around the rod-like structure. The second pathway, referred to as the 'cooperative formation mechanism' (Monnier *et al.*, 1993) emphasized the effect of the addition of silicate. In other words, the addition of silicate resulted in the ordering of the subsequent silicate-encaged surfactant micelles. Comparing the two pathways, the remarkable difference was whether the liquid crystal phase formed before or after the addition of silicate.

At the typical surfactant-silicate synthesis temperatures in the absence of silicates, an hexagonal phase is favored at surfactant concentrations between 25 and 70 wt.% for a CTAB-water solution (Auvray *et al.*, 1989; Monnier *et al.*, 1993), followed by the formation of a cubic phase and a lamellar phase at higher concentrations. MCM-41 was prepared successfully at a very low surfactant concentration of 2 wt.% in the experiment, which is not well explained by the first pathway in the LCT mechanism.

The organization of surfactant molecules into arrays at concentrations below the liquid crystal phase region is characterized by two critical micelle concentrations (*cmc*1 and *cmc*2), which represent the concentrations for the formation of spherical and rod-like micelles, respectively. At the lowest concentration of surfactants, the micelles formed are spherical or rod like. The sphere-to-rod transformation is strongly dependent on temperature, anion, and surfactant chain length. For CTAB, the transition concentration of sphere to rod-like micelle was 25 wt.% at 70ºC and 7−10 wt.% at room temperature (Huo *et al.*, 1994b). Only sphere micelles and isolated molecules existed in the surfactant solution containing CTAB at a concentration of 2 wt.%. The spherical micelle geometry was clearly not a structure-determining factor in the synthesis because the final hexagonal, lamellar, and cubic structures were not generated by spherical symmetry (Huo *et al.*, 1994b). Based on the analysis above, one can deduce that a pre-organized organic array was unnecessary, and perhaps unrelated to the final mesostructure of the product. A possible schematic model of MCM-41 formation is shown (Figure 7) and is based on a combination of proposed models (Beck *et al.*, 1992; Monnier *et al.*, 1993; Huo *et al.*, 1994b; Firouzi *et al.*, 1995) and on the experiment results.

Monnier *et al.* (1993) pointed out that, for dilute solutions, the important structure-determining factor was the role of the highly charged anionic inorganic species which controlled the surfactant geometry through charge-density matching and multi-dentate bonding. In the experiment, the multi-dentate charge density of preferentially polymerized silicates in the region of the CTAB-silicate interface, together with a double layer was responsible for the regularity of the resultant ordered MCM-41. The former determined the initial CTAB molecular siting and array possibilities and the latter controlled the wall thickness (Monnier *et al.*, 1993). According to the 'charge density matching' rule through a cooperative function (Figure 7b), the long chains of the CTAB phase preferred to close and organize, forming the favorable morphology in order to minimize the van der Waals forces of the CTAB molecules and to minimize the charge energies of silicates and CTAB. The organized structure then

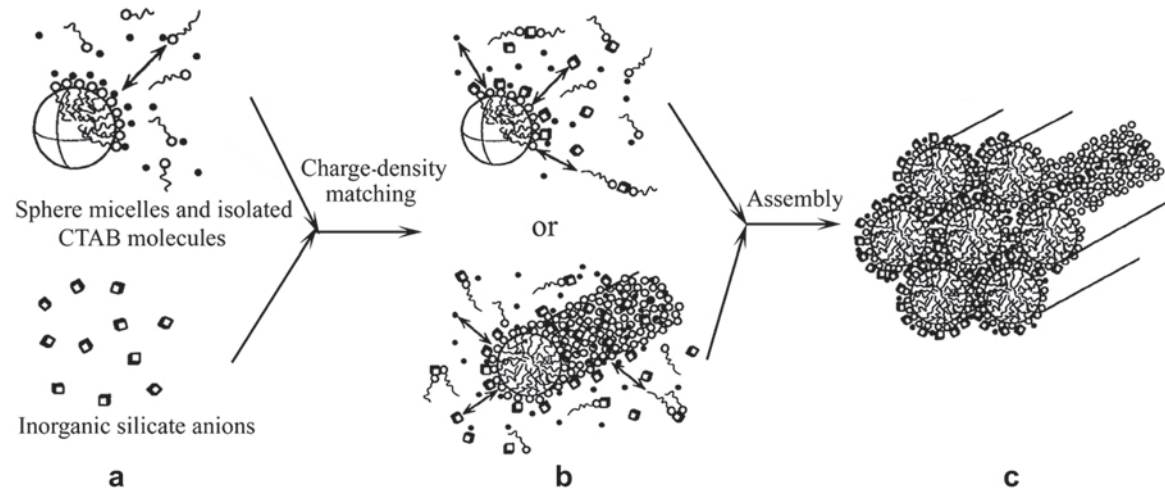

Figure 7. Schematic model of the possible formation of MCM-41.

underwent the assembly process to form the final ordered MCM-41 (Figure 7c). In the process of forming ordered MCM-41, charge-density matching, which governed the positions of the CTA^+ cations' array, combined with the degree of polymerization of the silicates, ultimately determined the resultant mesophase.

CONCLUSIONS

Porous silica (PS) and the mesoporous material MCM-41 were prepared from a single, ubiquitous silicate, talc, by a facile two-step method. PS, with a specific surface area of 260 m^2/g, a pore volume of 0.51 cm^3/g, and a bimodal pore-size distribution of 1.2 nm and 3.7 nm, was obtained through acid leaching after mechano-chemical treatment. The as-prepared porous silica could be used simultaneously as a source of Si for the fabrication of MCM-41with large surface area of 974 m^2/g, a large pore volume of 1.00 cm^3/g, and uniform pore-size distribution of 2.8 nm. The MCM-41 obtained had similar properties to that prepared using the direct synthesis route. Grinding played an important role in the whole synthesis process – reducing the particle size of the talc and weakening the Mg–OH bonds facilitated the subsequent leaching. Results from the ^{29}Si NMR and FTIR spectra demonstrated that acid leaching transformed $Si(SiO)_3OMg$ to $Si(SiO)_3(OH)$. Three distinct peaks located at −98, −102, and −108 ppm in the ^{29}Si NMR spectra of MCM-41 correspond to three different chemical environments of Si atoms: preserved layered structure $Si(SiO)_3OMg$, silanol Q^3 $Si(SiO)_3(OH)$ structure, and a three-dimensional cross-linked framework Q^4 $(Si(SiO)_4)$ structure. At a very low CTAB concentration (2 wt.%), the highly charged silicate species were important structure-determining factors in the process of forming ordered MCM-41. Charge-density matching governed the interaction between CTA^+ cations and polymerized silicates. The surfactant array and the degree of polymerization of silicates ultimately determined the resultant mesostructure. The strategy reported here is of fundamental importance because it opens new possibilities for the development of other kinds of porous materials. The realization of 'One common source, two advanced materials' will undoubtedly lead to industrial applications in the future.

ACKNOWLEDGMENTS

This work was supported by the National Natural Science Foundation of China (50774095, 50304014), the Program for New Century Excellent Talents in University (NCET-05-0695), the Excellent Youth Foundation of Central South University and the Program for New Century 121 Excellent Talents in Hunan Province (05-030119).

REFERENCES

Auvray, X., Petipas, C., Anthore, R., Rico, I., and Lattes, A. (1989) X-ray diffraction study of mesophases of cetyltrimethylammonium bromide in water, formamide, and glycerol. *Journal of Physical Chemistry*, **93**, 7458–7464.

Azaïs, T., Tourné-Péteilh, C., Aussenac, F., Baccile, N., Coelho, C., Devoisselle, J-M., and Babonneau, F. (2006) Solid-state NMR study of ibuprofen confined in MCM-41 material. *Chemistry of Materials*, **18**, 6382–6390.

Aznar, A.J., Gutiérrez, E., Díaz, P., Alvarez, A., and Poncelet, G. (1996) Silica from sepiolite: preparation, textural properties, and use as support to catalysts. *Microporous Materials*, **6**, 104–114.

Baccile, N., Laurent, G., Bonhomme, C., Innocenzi, P., and Babonneau, F. (2007) Solid-state NMR characterization of the surfactant-silica interface in templated silicas: acidic versus basic conditions. *Chemistry of Materials*, **19**, 1343–1354.

Beck, J.S., Vartuli, J.C., Roth, W.J., Leonowicz, M.E., Kresge, C.T., Schmitt, K.D., Chu, C.T-W., Oison, D.H., Sheppard, E.W., McCullen, S.B., Higgins, J.B., and Schlenker, J.L. (1992) A new family of mesoporous molecular sieves prepared with liquid crystal templates. *Journal of the*

American Chemical Society, **114**, 10834–10843.

Bisio, C., Gatti, G., Boccaleri, E., Marchese, L., Bertinetti, L. (2008) On the acidity of saponite materials: a combined HRTEM, FTIR,, and Solid-State NMR Study. *Langmuir*, **24**, 2808–2819.

Boissière, C., Larbot, A., and Prouzet, E. (2000) Synthesis of mesoporous MSU-*X* materials using inexpensive silica sources. *Chemistry of Materials*, **12**, 1937–1940.

Cai, Y., Kumar, R., Huang, W., Trewyn, B.G., Wiench, J., Pruski, M., and Lin, V.S-Y. (2007) Mesoporous aluminum silicate catalyst with single-type active sites: characterization by solid-state NMR and studies of reactivity for claisen rearrangement reactions. *Journal of Physical Chemistry C*, **111**, 1480–1486.

Coasne, B., Galarneau, A., Renzo, F.D., and Pellenq, R.J.M. (2006) Gas adsorption in mesoporous micelle-templated silicas: MCM-41, MCM-48, and SBA-15. *Langmuir*, **22**, 11097–11105.

Corma, A. (1997) From microporous to mesoporous molecular sieve materials and their use in catalysis. *Chemical Reviews*, **97**, 2373–2419.

Davis, M.E. (2002) Ordered porous materials for emerging applications. *Nature*, **417**, 813–821.

Firouzi, A., Kumar, D., Bull, L.M., Besier, T., Sieger, P., Huo, Q., Walker, S.A., Zasadzinski, J.A., Glinka, C., Nicol, J., Margolese, D., Stucky, G.D., and Chmelka, B.F. (1995) Cooperative organization of inorganic-surfactant and biomimetic assemblies. *Science*, **267**, 1138–1143.

Huo, Q., Margolese, D.I., Ciesla, U., Demuth, D., Feng, P., Gier, T., Sieger, P., Firouzi, A., Chmelka, B., Schûth, F., and Stucky, G.D. (1994a) Organization of organic-molecules with inorganic molecular-species into nanocomposite biphase arrays. *Chemistry of Materials*, **6**, 1176–1191.

Huo, Q., Margolese, D.I., Ciesla, U., Feng, P., Sieger, P., Leon, R., Petroff, P., Schûth, F., and Stucky, G.D. (1994b) Generalized synthesis of periodic surfactant/inorganic composite materials. *Nature*, **368**, 317–321.

Inagaki, S., Fukushima, Y., and Kuroda, K. (1993) Synthesis of highly ordered mesoporous materials from a layered polysilicate. *Journal of Chemical Society, Chemical Communications*, 680–682.

Jin, S., Qiu, G., Xiao, F., Chang, Y., and Wan, C. (2007) Investigation of the structural characterization of mesoporous molecular sieves MCM-41 from sepiolite. *Journal of American Ceramic Society*, **90**, 957–961.

Kaviratna, H., and Pinnavaia, T. (1994) Acid hydrolysis of octahedral Mg^{2+} sites in 2:1 layered silicates: an assessment of edge attack and gallery access mechanisms. *Clays and Clay Minerals*, **42**, 717–723.

Kinsey, R.A., Kirkpatrick, R.J., Hower, J., Smith, K.A., and Oldfield, E. (1985) High resolution aluminum-27 and silicon-29 nuclear magnetic resonance spectroscopic study of layer silicates, including clay minerals. *American Mineralogist*, **70**, 537–548.

Kosuge, K., Shimada, K., and Tsunashima, A. (1995) Micropore formation by acid treatment of antigorite. *Chemistry of Materials*, **7**, 2241–2246.

Kosuge, K., Kikukawa, N., and Takemori, M. (2004) One-step preparation of porous silica spheres from sodium silicate using triblock copolymer templating. *Chemistry of Materials*, **16**, 4181–4186.

Kresge, C.T., Leonowicz, M.E., Roth, W.J., Vartuli, J.C., and Beck, J.S. (1992) Ordered mesoporous molecular sieves synthesized by a liquid-crystal template mechanism. *Nature*, **359**, 710–712.

Laughlin, R.G. (1991) Cationic surfactants: physical chemistry. *Surfactant Science Series*, **37**, 1.

Linssen, T., Cool, P., Baroudi, M., Cassiers, K., Vansant, E.F., Lebedev, O., and Landuyt, J.V. (2002) Leached natural saponite as the silicate source in the synthesis of aluminosilicate hexagonal mesoporous materials. *Journal of Physical Chemistry B*, **106**, 4470–4476.

Linssen, T., Cassiers, K., Cool, P., Lebedev, O., Whittaker, A., and Vansant, E.F. (2003) Physicochemical and structural characterization of mesoporous aluminosilicates synthesized from leached saponite with additional aluminum incorporation. *Chemistry of Materials*, **15**, 4863–4873.

Lubguban, Jr., J., Kurate, Y., Inokuma, T., and Hasegawa, S. (2000) Thermal stability and breakdown strength of carbon-doped SiO_2: F films prepared by plasma-enhanced chemical vapor deposition method. *Journal of Applied Physics*, **87**, 3715–3722.

MacKenzie, K.J.D., Okada, K., and Temuujin, J. (2004) Nanoporous inorganic materials from mineral templates. *Current Applied Physics*, **4**, 167–170.

Madhusoodana, C.D., Kameshima, Y., Nakajima, A., Okada, K., Kogure, T., and MacKenzie, K.J.D. (2006) Synthesis of high surface area Al-containing mesoporous silica from calcined and acid-leached kaolinites as the precursors. *Journal of Colloid and Interface Science*, **297**, 724–731.

Maqueda, C., Romero, A.S., Morillo, E., and Pérez-Rodríguez, J.L. (2007) Effect of grinding on the preparation of porous materials by acid-leached vermiculite. *Journal of Physics and Chemistry of Solids*, **68**, 1220–1224.

Miao, S., Liu, Z., Ma, H., Han, B., Du, J., Sun, Z., and Miao, Z. (2005) Synthesis and characterization of mesoporous aluminosilicate molecular sieve from K-feldspar. *Microporous and Mesoporous Materials*, **83**, 277–282.

Mokaya, R. (1999) Improving the stability of mesoporous MCM-41 silica via thicker more highly condensed pore walls. *Journal of Physical Chemistry B*, **103**, 10204–10208.

Monnier, A., Schûth, F., Huo, Q., Kumar, D., Margolese, D., Maxwell, R.S., Stucky, G.D., Krishnamurty, M., Petroff, P., Firouzi, A., Janicke, M., and Chmelka, B.F. (1993) Cooperative formation of inorganic-organic interfaces in the synthesis of silicate mesostrucures. *Science*, **261**, 1299–1303.

Mukhopadhyay, K., Sarkar, B.R., and Chaudhari, R.V. (2002) Anchored Pd complex in MCM-41 and MCM-48: novel heterogeneous catalysts for hydrocarboxylation of aryl olefins and alcohols. *Journal of American Chemical Society*, **124**, 9692–9693.

Okada, K., Shimai, A., Takei, T., Hayashi, S., Yasumori, A., and MacKenzie, K.J.D. (1998) Preparation of microporous silica from metakaolinite by selective leaching method. *Microporous and Mesoporous Materials*, **21**, 289–296.

Okada, K., Nakazawa, N., Kameshima, Y., Yasumori, A., Tumuujin, J., MacKenzie, K.J.D., and Smith, M. (2002) Preparation and porous properties of materials prepared by selective leaching of phlogopite. *Clays and Clay Minerals*, **50**, 624–632.

Okada, K., Temuujin, J., Kameshima, Y., and MacKenzie, K.J.D. (2003) Selective acid leaching of talc. *Clay Science*, **12**, 159–165.

Okada, K., Arimitsu, N., Kameshima, Y., Nakajima, A., and MacKenzie, K.J.D. (2005) Preparation of porous silica from chlorite by selective acid leaching. *Applied Clay Science*, **30**, 116–124.

Okada, K., Yoshizaki, H., Kameshima, Y., Nakajima, A., and Madhusoodana, C.D. (2007) Synthesis and characterization of mesoporous silica from selectively acid-treated saponite as the precursors. *Journal of Colloid and Interface Science*, **314**, 176–183.

Pauly, T.R., Petkov, V., Liu, Y., Billinge, S.J.L., and Pinnavaia, T.J. (2002) Role of framework sodium versus local framework structure in determining the hydrothermal stability of MCM-41 mesostructures. *Journal of the American Chemical Society*, **124**, 97–103.

Sánchez-Soto, P.J., Wiewióra, A., Avilés, M.A., Justo, A., Pérez-Maqueda, L.A., Pérez-Rodríguez, J.L., and Bylina, P. (1997) Talc from Puebla de Lillo, Spain. II. Effect of dry grinding on particle size and shape. *Applied Clay Science*, **12**, 297–312.

Shenderovich, H.G., Mauder, D., Akcakayiran, D., Buntkowsky, G., Limbach, H-H., and Findenegg, G.H. (2007) NMR provides checklist of generic properties for atomic-scale models of periodic mesoporous silicas. *Journal of Physical Chemistry B*, **111**, 12088–12096.

Suquet, H. (1989) Effects of dry grinding and leaching of the crystal structure of chrysotile. *Clays and Clay Minerals*, **37**, 439-445.

Temuujin, J., Okada, K., Mackenzie, K.J.D., and Jadambaa, T.S. (2001a) Characterization of porous silica prepared from mechanically amorphized kaolinite by selective leaching. *Powder Technology*, **121**, 259–262.

Temuujin, J., Burmaa, G., and Amgalan, J. (2001b) Preparation of porous silica from mechanically activated kaolinite. *Journal of Porous Materials*, **8**, 233–238.

Temuujin, J., Okada, K., Jadambaa, T.S., Mackenzie, K.J.D., and Amarsanaa, J. (2002) Effect of grinding on the preparation of porous material from talc by selective leaching. *Journal of Materials Science Letters*, **21**, 1607–1609.

Temuujin, J., Okada, K., and MacKenzie, K.J.D. (2003a) Preparation of porous silica from vermiculite by selective leaching. *Applied Clay Science*, **22**, 187–195.

Temuujin, J., Okada, K., Jadambaa, T.S., MacKenzie, K.J.D., and Amarsanaa, J. (2003b) Effect of grinding on the leaching behaviour of pyrophyllite. *Journal of the European Ceramic Society*, **23**, 1277–1282.

Trébosc, J., Wiench, J.W., Huh, S., Lin, V.S-Y., and Pruski, M.J. (2005) Solid-state NMR study of MCM-41-type mesoporous silica nanoparticles. *Journal of the American Chemical Society*, **127**, 3057–3068.

Vallet-Regi, M., Rámila, A., del Real, R.P., and Pérez-Pariente, J. (2001) A new property of MCM-41: drug delivery system. *Chemistry of Materials*, **13**, 308–311.

Vicente, M.A., Suárez, M., López-González, J. de D., and Bañares-Muñoz, M.A. (1996) Characterization, surface area, and porosity analyses of the solids obtained by acid leaching of a saponite. *Langmuir*, **12**, 566–572.

Warren, A.C., Messina, L.C., Slaughter, L.S., Kamperman, M., Zhou, Q., Gruner, S.M., DiSalvo, F.J., and Wiesner, U. (2008) Ordered mesoporous materials from metal nanoparticle-block copolymer self-assembly. *Science*, **320**, 1748–1753.

Xu, J., Luan, Z., He, H., Zhou, W., and Kevan, L. (1998) A reliable synthesis of cubic mesoporous MCM-48 molecular sieve. *Chemistry of Materials*, **10**, 3690–3698.

Yanagisawa, T., Shimizu, T., Kuroda, K., and Kato, C. (1990) The preparation of alkyltrimethylammonium-kanemite complexes and their conversion to microporous materials. *Bulletin of the Chemical Society of Japan*, **63**, 988–992.

Yang, H., Du, C., Hu, Y., Jin, S., Yang, W., Tang, A., and Avvakumov, E.G. (2006) Preparation of porous material from talc by mechanochemical treatment and subsequent leaching. *Applied Clay Science*, **31**, 290–297.

Zhao, D.Y., Feng, J.L., Huo, Q.S., Melosh, N., Fredrickson, G.H., Chmelka, B.F., and Stucky, G.D. (1998) Triblock copolymer syntheses of mesoporous silica with periodic 50 to 300 angstrom pores. *Science*, **279**, 548–552.

(*Received 17 October 2008; revised 19 January 2009; Ms. 0214; A.E. S. Petit*)